# The Effect of Axial Mg Ligation on the Geometry and Spin Density Distribution of Chlorophyll and Bacteriochlorophyll Cation Free Radical Models: A Density Functional Study

**Patrick J. O'Malley* and Simon J. Collins**

*Contribution from the Department of Chemistry, UMIST, Manchester, M60 1QD, UK*

*Received February 26, 2001*

**Abstract:** Density functional calculations are performed on models of chlorophyll and bacteriochlorophyll to examine the effect of Mg ligation on the geometry and spin density distribution of the cation free radicals formed. It is shown that, whereas the properties of the bacteriochlorophyll model can be explained on the basis of the electron density distribution of the highest occupied molecular orbital (HOMO), for the chlorophyll model the geometry and spin density properties of the ligated species do not follow this trend. For the ligated chlorophyll models it is shown that, due to the closeness in energy of the HOMO and HOMO-1 orbitals, a Jahn−Teller distortion occurs on one-electron oxidation, leading to an admixed hybrid orbital for the cation radical form. Orbital mixing is shown to lead to significant changes in the geometry and spin density distribution of the cation free radical formed. It is also shown that orbital mixing does not lead to an increase in the magnitude of the $^{14}N$ hyperfine couplings thereby invalidating reports in the literature which have dismissed mixed orbital states for the primary donor cation radicals of photosynthetic reaction centers based on this criterion.

## Introduction

Porphyrins and (bacterio)chlorins play important roles in many biological electron-transfer processes.[1] Initial electron transfer in photosynthesis leads to one-electron oxidation of the primary donor chlorophyll(bacteriochlorophyll) in plant and bacterial photosynthesis.[2] The electronic structure of the oxidized primary donor free radical can provide an important insight into the mechanism of initial electron transfer, and hence the cation radical so formed has been the subject of numerous experimental magnetic resonance studies.[3−10] While the bacterial primary donor free radical is currently thought to have a delocalized spin density over the two bacteriochlorophylls constituting the primary donors,[3,4,6] both delocalized and monomer models have been proposed for the higher plant primary donor radicals of Photosystem I(PS I) and Photosystem II(PS II).[5,7,8,9,10] The delocalized models assume a situation similar to that occurring for the bacterial systems with partial delocalization of the spin density over two chlorophyll-type molecules. In the modified monomer model, as originally proposed,[5,7] the altered spin density distribution for the primary donor cation free radical results from orbital admixing between the HOMO and HOMO-1 orbitals. This admixing was principally attributed to the effect of ligation by the protein of the central Mg. It has been argued in the literature that it is possible to distinguish between monomer or delocalized dimer models on the basis of the measured $^{14}N$ hyperfine coupling. For delocalized dimer models a reduction in $^{14}N$ hyperfine coupling compared with the monomer is expected, whereas it has been argued[10] that a mixed orbital model would result in a substantial increase in the $^{14}N$ isotropic hyperfine couplings. On the basis of this criterion it has been suggested[10] that the mixed orbital model can be eliminated for both bacterial and plant Photosystem I donor radicals as no such increase in nitrogen hyperfine couplings has been observed experimentally.

In this contribution we use density functional calculations on model (bacterio)chlorophyll systems to demonstrate that axial ligation does indeed induce orbital mixing for chlorophyll model systems, leading to significant alterations of geometry and spin density distributions. No such mixing is thus far predicted to occur for the bacteriochlorophyll models. Calculation of the isotropic $^{14}N$ isotropic hyperfine couplings shows that in contrast to recent reports[10] a mixed orbital state for chlorophyll cation radicals does not lead to an increased magnitude for the $^{14}N$ isotropic hyperfine couplings.

## Methods

The molecular structures of chlorophyll *a* and bacteriochlorophyll *a* are shown in Figure 1. The models of chlorophyll *a* and bacteriochlorophyll *a* used are shown in Figure 2. Groups peripheral to the main aromatic system are replaced by hydrogen atoms in the models to make computational studies feasible. The singly ligated state is simulated by one water molecule ligated via its oxygen atom to the

(1) (a) Frew, J. E.; Jones, P. *Adv. Inorg. Bioinorg. Mech.* **1984**, *3*, 175. (b) Scheer, H., Ed. *Chlorophylls*; CRC: Boca Raton, FL, 1991.
(2) Brettel, K. *Biochim. Biophys.* Acta **1997**, *1318*, 322.
(3) Norris, J. R.; Scheer, H.; Katz, J. *Proc. Natl. Acad. Sci. U.S.A.* **1974**, *71*, 4897.
(4) Feher, G.; Hoff, A. J.; Isaacson, R. A.; Ackerson, L. C. *Ann. N.Y. Acad. Sci.* **1975**, *244*, 239.
(5) Davis, M. S.; Forman, A.; Fajer, J. *Proc. Natl. Acad. Sci. U.S.A.* **1979**, *76*, 4170.
(6) Lendzian, F.; Huber, M.; Isaacson, R. A.; Endeward, B.; Plato, M.; Bonigk, B.; Möbius, K.; Lubitz, W.; Feher, G. *Biochim. Biophys. Acta* **1993**, *1183*, 139.
(7) O'Malley, P. J.; Babcock, G. T. *Proc. Natl. Acad. Sci. U.S.A.* **1984**, *81*, 1098.
(8) Rigby, S. E. J.; Nugent, J. H. A.; O'Malley, P. J. *Biochemistry* **1994**, *33*, 10043.
(9) Mac, M.; Bowlby, N. R.; Babcock, G. T.; McCracken, J. *J. Am. Chem. Soc.* **1998**, *120*, 13215.
(10) Käss, H.; Fromme, P.; Witt, H.; Lubitz, W. *J. Phys. Chem. B* **2001**, *105*, 1225.

10.1021/ja010522u CCC: $20.00 
Published on Web 10/12/2001

**Table 1.** Selected Optimized Bond Lengths, in Å, for the Neutral Models of Figure 2[a]

| bond | BChl | BChl-1w | BChl-2w | Chl | Chl-1w | Chl-2w |
|---|---|---|---|---|---|---|
| C1−C2 | 1.425(+0.023) | 1.426(+0.024) | 1.428(+0.024) | 1.437(+0.004) | 1.440(+0.003) | 1.442(+0.002) |
| C2−C3 | 1.383(−0.017) | 1.385(−0.019) | 1.386(−0.018) | 1.377(−0.007) | 1.376(−0.006) | 1.377(−0.002) |
| C3−C4 | 1.451(+0.016) | 1.452(+0.017) | 1.454(+0.018) | 1.463(+0.021) | 1.465(+0.019) | 1.468(+0.013) |
| C1−N21 | 1.381(−0.004) | 1.380(−0.004) | 1.378(−0.004) | 1.365(+0.008) | 1.362(+0.004) | 1.362(−0.011) |
| N21−C4 | 1.370(−0.001) | 1.368((−0.002) | 1.364(−0.004) | 1.382(−0.011) | 1.379(−0.004) | 1.375(+0.009) |
| C4−C5 | 1.408(−0.006) | 1.413(−0.009) | 1.418(−0.007) | 1.391(+0.004) | 1.391(−0.001) | 1.397(−0.013) |
| C5−C6 | 1.390(+0.007) | 1.390(+0.007) | 1.394(+0.006) | 1.413(−0.004) | 1.415(+0.001) | 1.418(+0.017) |
| C6−N22 | 1.358(+0.003) | 1.358+0.002) | 1.357(+0.003) | 1.367(−0.003) | 1.363(−0.005) | 1.366(−0.018) |
| N22−C9 | 1.368(−0.003) | 1.366(−0.004) | 1.366(−0.006) | 1.380(−0.002) | 1.378(+0.003) | 1.379(+0.009) |
| C9−C10 | 1.386(+0.014) | 1.388(+0.013) | 1.391(+0.015) | 1.406(−0.004) | 1.405(−0.009) | 1.411(−0.017) |
| C10−C11 | 1.411(−0.013) | 1.414(−0.014) | 1.419(−0.015) | 1.398(+0.005) | 1.401(+0.009) | 1.405(+0.020) |
| C11−N23 | 1.384(−0.003) | 1.382(−0.003) | 1.378(−0.004) | 1.393(−0.014) | 1.393(−0.019) | 1.390(−0.025) |
| N23−C14 | 1.348(−0.002) | 1.347(−0.002) | 1.344(−0.002) | 1.337(+0.007) | 1.337(+0.011) | 1.336(+0.012) |
| C14−C15 | 1.406(−0.005) | 1.408(−0.006) | 1.410(−0.005) | 1.413(−0.017) | 1.417(−0.024) | 1.417(−0.022) |
| C15−C16 | 1.384(+0.008) | 1.387(+0.006) | 1.391(+0.006) | 1.378(+0.021) | 1.379(+0.029) | 1.385(+0.040) |
| C16−N24 | 1.370(+0.004) | 1.365(+0.005) | 1.361(+0.006) | 1.376(+0.009) | 1.375(−0.020) | 1.367(−0.031) |
| N24−C19 | 1.359(−0.003) | 1.358(−0.004) | 1.353(−0.005) | 1.359(+0.009) | 1.357(+0.015) | 1.350(+0.031) |
| C19−C20 | 1.488(+0.014) | 1.389(+0.014) | 1.394(+0.016) | 1.388(+0.004) | 1.390(−0.004) | 1.396(−0.018) |
| C20−C1 | 1.408(−0.011) | 1.412(−0.013) | 1.413(−0.013) | 1.412(−0.005) | 1.414(0.000) | 1.415(+0.019) |

[a] The changes occurring on one-electron oxidation to the cation radical form are given in brackets.

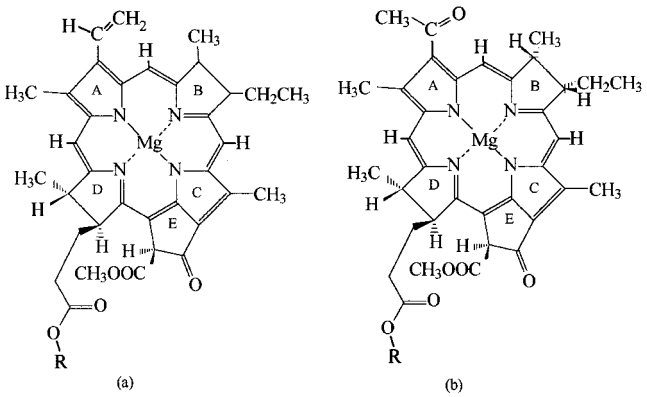

**Figure 1.** Molecular structures for (a) chlorophyll *a* and (b) bacteriochlorophyll *a*

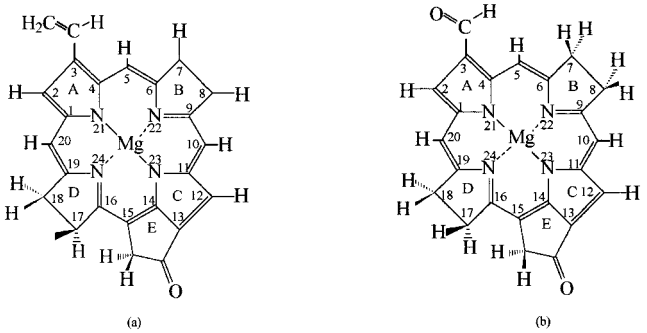

**Figure 2.** Models used for density functional calculations. (a) Chl and (b) BChl. Water was used to simulate central Mg ligation. A single water molecule ligated to the central Mg model is notated (B)Chl-1w, while for two water molecules ligated to the central Mg, on opposite sides of the ring, the notation used is (B)Chl-2w.

central Mg, Chl/BChl-1w, whereas double ligation is modeled by two such water molecules, on opposite sides of the ring plane, Chl/BChl-2w. All geometry optimizations were performed using standard procedures of Gaussian 98.[12] The B3LYP functional was used throughout in combination with the 6-31G(d) basis set. Restricted Kohn−Sham was used for the closed shell neutral models, and unrestricted Kohn−Sham was used for the open shell radical forms.

## Results and Discussion

The principal bond distances for BChl/BChl$^{\bullet+}$, BChl-1w/BChl-1w$^{\bullet+}$ and BChl-2w/BChl-2w$^{\bullet+}$ and their chlorophyll counterparts, Chl/Chl$^{\bullet+}$, Chl-1w/Chl-1w$^{\bullet+}$, and Chl-2w/Chl-2w$^{\bullet+}$ are given in Table 1. Oxidation of the pigments occurs by electron removal from the HOMO orbital, Figure 3, of the neutral pigment. To a first approximation, any bond length changes should therefore reflect the electron density pattern of this orbital, with those bonds in bonding regions being weakened/lengthened, while those corresponding to antibonding regions should be strengthened/shortened. For nonbonding regions no significant bond-order changes are expected to occur on oxidation. These expectations are borne out by the BChl models. For example, for the A ring, the geometry changes observed on oxidation for BChl are in accord with this; oxidation leads to a bond length increase for the C1−C2 and C3−C4 bonds, whereas C2−C3 decreases, reflecting the bonding HOMO nature of C1−C2/C3−C4 and the corresponding antibonding nature of C2−C3, Figure 3. Significant bond length changes occur also for the C9−C10, C10−C11 and C19−C20, C20−C1 bonds. Here again the bonding nature of the HOMO for C9−C10 and C19−C20 leads to a lengthening of both bonds on oxidation, while the antibonding nature of C10−C11 and C20−C1 leads to a shortening of both bonds on oxidation. For those bonds situated in predominantly nonbonding regions no significant bond length changes are expected to occur on oxidation, and this is borne out by the calculated BChl values in Table 1. From Table 1 we can see that for the BChl model single or double ligation has no significant influence on the bond length changes occurring on one-electron oxidation of the pigment. For the nonligated Chl model the bond length changes occurring on oxidation are again reasonably well accounted for on the basis of the bonding/antibonding/nonbonding nature of the HOMO. For Chl-1w and Chl-2w, however, the bond length changes occurring on oxidation do not follow from the nature of the HOMO. For Chl-2w in particular an alternating pattern of bond length changes is predicted to occur around the chlorin ring. These bond length alternations cannot be explained on the basis of the neutral HOMO, which is mainly nonbonding in this region, Figure 4. For the Chl-1w and in particular the Chl-2w model oxidation appears to lead to a significant rearrangement of the electron density in the ring. Inspection of the HOMO

(11) (a) Prendergast, K.; Spiro, T. G. *J. Phys. Chem.* **1991**, *95*, 9728. (b) Barzilay, C. M.; Sibilia, S. A.; Spiro, T. G.; Gross, Z. *Chem. Eur. J.* **1995**, *4*, 222 (c) Blackwood, M. E., Jr.; Spiro, T. G. *J. Phys. Chem. B* **1997**, *101*, 8363.

(12) Frisch, M. J.; Trucks G. W.; Schlegel, H. B.; Gill, P. W.; Johnson, B. G.; Wong, M. W.; Foresman, J. B.; Tomasi, J.; Barone, V.; Adamo, C.; Robb, M. A.; Head-Gordon, M.; Replogle, E. S.; Gomperts, R.; Andres, J. L.; Raghvachari, K.; Binkley, J. S.; Gonzalez, C.; Martin, R. L.; Fox, D. J.; Defrees, D. J.; Baker, J.; Gonzalez, C.; Martin, R. L.; Fox, D. J.; Defrees, D. J.; Baker, J.; Stewart, J. J. P.; Pople, J. A. *Gaussian 98*; Gaussian Inc.: Pittsburgh, PA, 1998

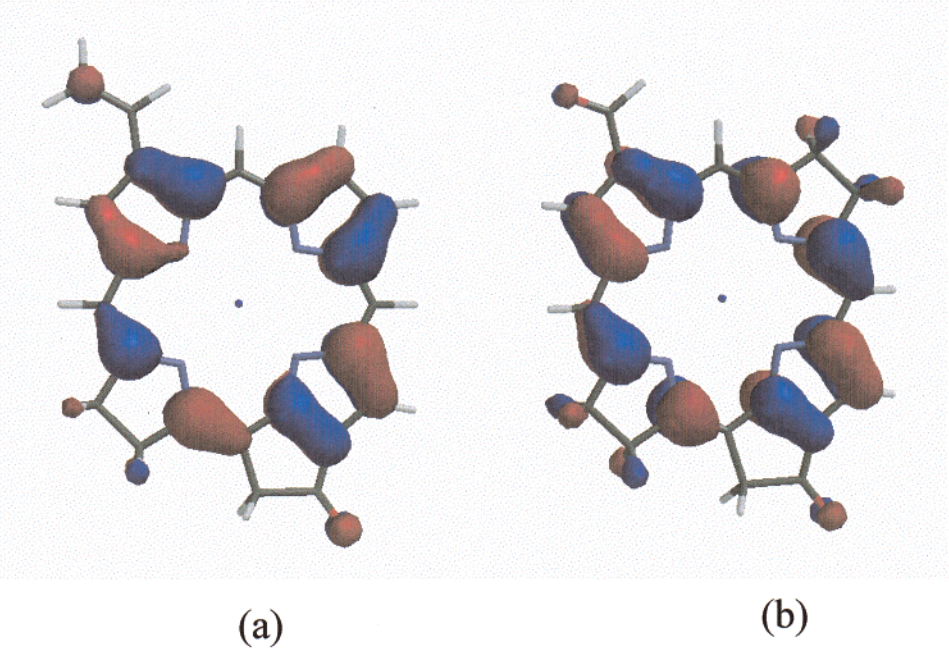


**Figure 3.** HOMO electron density surfaces, 0.03 e/au$^3$ for (a) Chl and (b) BChl.

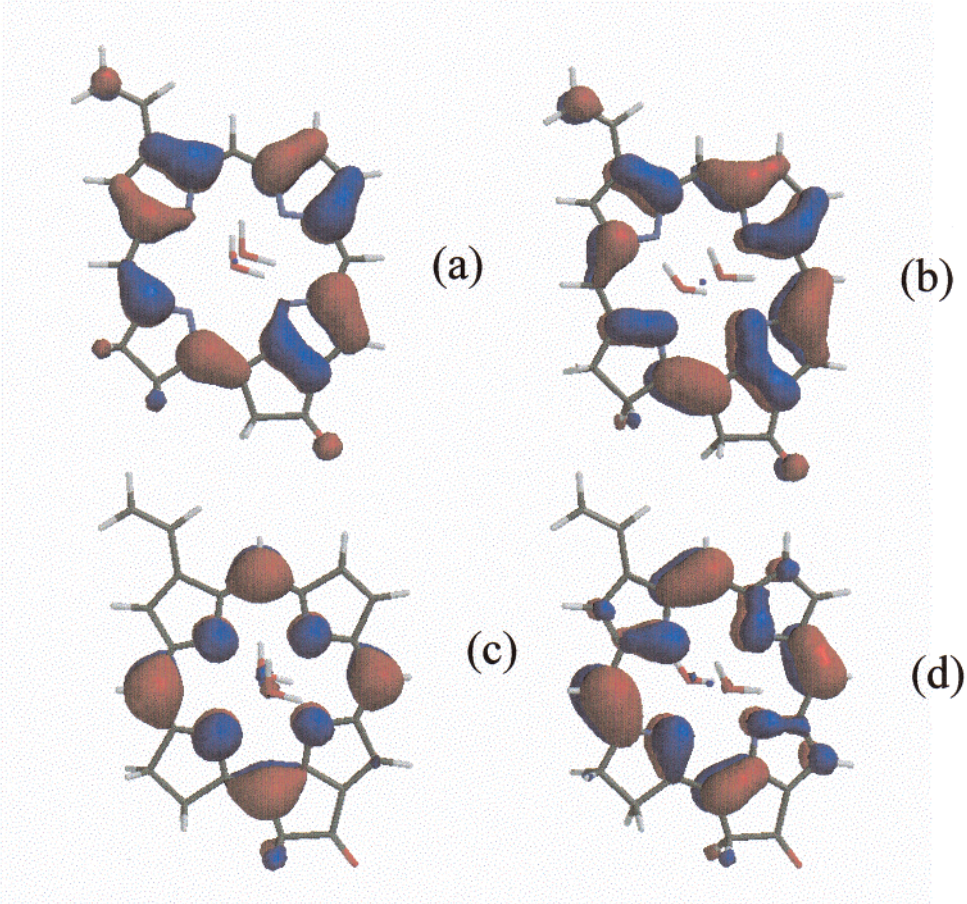


**Figure 4.** Comparison of HOMO and HOMO-1 orbital for the neutral Chl-2w model (a and c) with the HOMO and HOMO-1 orbitals of the cation free radical form (b and d). All orbitals are contoured at 0.03 e/au$^3$.

and HOMO-1 orbitals for the neutral and cation radicals of Chl-2w and BChl-2w presented in Figures4 and 5, respectively, provides an explanation of this trend. For BChl-2w, Figure 5, the HOMO and HOMO-1 orbitals for the oxidized form are similar to those for the neutral unoxidized form, and hence, as described above, geometry changes on oxidation are determined by the bonding/antibonding/nonbonding nature of the HOMO. For Chl-2w, however, a significant difference in the electron density pattern for the HOMO and HOMO-1 orbitals of the neutral and oxidized species are revealed in Figure 4. Inspection of the HOMO and HOMO-1 orbitals for Chl-2w$^{\bullet+}$ shows that they can be ascribed to admixing of the HOMO and HOMO-1

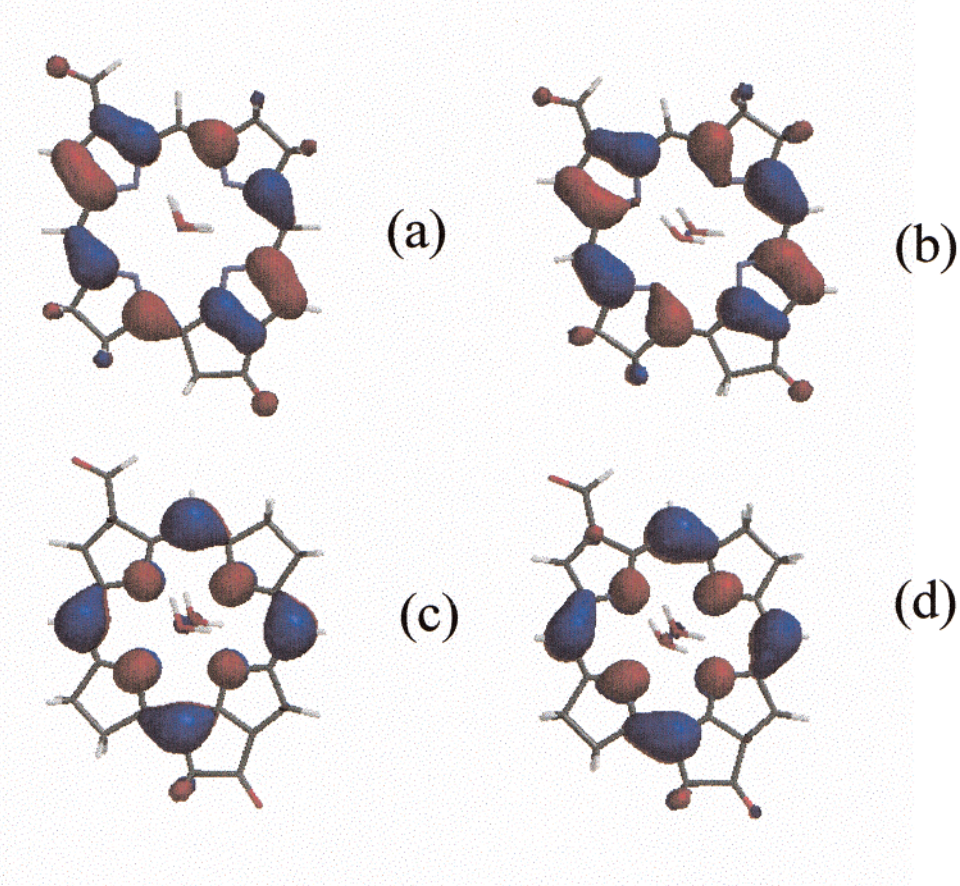


**Figure 5.** Comparison of HOMO and HOMO-1 for the neutral BChl-2w model (a and c) with the HOMO and HOMO-1 orbitals of the cation free radical form (b and d). All orbitals are contoured at 0.03 e/au$^3$.

orbitals of the neutral pigment. In this case oxidation of the neutral pigment brings about a Jahn−Teller type distortion of the chlorin ring caused by the closeness in energy of the HOMO and HOMO-1 orbitals.[13] The resultant mixed orbitals, arising, now have an electron density significantly altered from that of the neutral pigment. In particular the doubly occupied HOMO-1 orbital of the oxidized cation, Figure 4d, has now alternating bonding/antibonding regions along the main chlorin ring system compared with the mainly nonbonding situation for this orbital in the neutral pigment. Hence, for the oxidized molecule one can predict alternate shortening and lengthening of the respective bonds. This is indeed what is observed in Table 1 for the Chl-2w$^{\bullet+}$ model. It is of interest that a very similar alternation of bond distances has been noted previously for the substituted porphyrin, ZnP$^{\bullet+}$.[11a] This has been attributed to a mixed frontier orbital caused by a Jahn−Teller distortion of the framework. In this case structural determinations for the cation radical confirms such bond alternations around the porphyrin ring.[14] From our model studies here we infer a similar situation arises for chlorophyll in the ligated state.

The calculated spin populations for the nitrogen, magnesium, and methine carbons are shown in Table 2, and the corresponding calculated $^{14}$N, $^{1}$H, and $^{26}$Mg isotropic hyperfine couplings are given in Table 3. Mg ligation brings about a significant change in spin population and hyperfine coupling for the Chl models. No significant changes are noted for the bacterial models. While the geometry changes for Chl-2w$^{\bullet+}$ point to a Jahn−Teller distortion with associated orbital mixing, it is clear from the spin populations and hyperfine couplings of Tables 2 and 3 that orbital mixing, albeit to a lesser degree, is occurring for Chl-1w$^{\bullet+}$ as well. In the absence of orbital mixing, that is the bacterial pigment case, the spin density mirrors the electron

**Table 2.** Spin Populations for the Cation Radical Forms of the Figure 2 Models

| position | BChl$^{\bullet+}$ | BChl-1w$^{\bullet+}$ | BChl-2w$^{\bullet+}$ | Chl$^{\bullet+}$ | Chl-1w$^{\bullet+}$ | Chl-2w$^{\bullet+}$ |
|---|---|---|---|---|---|---|
| N21 | −0.047 | −0.048 | −0.048 | −0.038 | −0.047 | −0.027 |
| N22 | −0.064 | −0.063 | −0.059 | −0.066 | −0.060 | −0.003 |
| N23 | −0.049 | −0.049 | −0.051 | −0.038 | −0.020 | 0.056 |
| N24 | −0.069 | −0.072 | −0.076 | −0.040 | −0.025 | 0.058 |
| C5 | −0.082 | −0.081 | −0.079 | −0.112 | −0.107 | −0.018 |
| C10 | −0.069 | −0.065 | −0.060 | −0.123 | −0.099 | 0.033 |
| C15 | −0.094 | −0.094 | −0.099 | −0.015 | 0.041 | 0.226 |
| C20 | −0.070 | −0.071 | −0.064 | −0.061 | −0.064 | −0.002 |
| Mg | 0.006 | 0.005 | 0.003 | 0.005 | 0.003 | −0.002 |

**Table 3.** $^{13}$C, $^{14}$N, and $^{25}$Mg Isotropic Hyperfine Couplings for the Cation Radical Forms of the Figure 2 Models

| position | BChl$^{\bullet+}$ | BChl-1w$^{\bullet+}$ | BChl-2w$^{\bullet+}$ | Chl$^{\bullet+}$ | Chl-1w$^{\bullet+}$ | Chl-2w$^{\bullet+}$ |
|---|---|---|---|---|---|---|
| N21 | −2.6 | −2.6 | −2.5 | −2.1 | −2.5 | −1.5 |
| N22 | −3.6 | −3.5 | −3.2 | −3.5 | −3.2 | −0.4 |
| N23 | −2.7 | −2.6 | −2.6 | −2.1 | −1.2 | 2.4 |
| N24 | −3.9 | −4.0 | −4.1 | −2.4 | −1.5 | 2.6 |
| C5 | −14.7 | −14.6 | −14.4 | −18.2 | −17.4 | −5.7 |
| C10 | −13.8 | −13.2 | −12.7 | −19.7 | −15.5 | 0.6 |
| C15 | −16.0 | −16.0 | −16.8 | −6.5 | 0.2 | 24.0 |
| C20 | −13.3 | −13.6 | −12.8 | −11.7 | −12.0 | −3.3 |
| Mg | −0.4 | −0.5 | −0.4 | −0.4 | −0.3 | 0.4 |

(13) For the chlorophyll models the calculated difference in orbital energies for the HOMO and HOMO-1 of the neutral Chl model is 0.19 eV. For Chl-2w this energy difference is reduced to 0.03 eV. For the bacteriochlorophyll models the corresponding energy differences are 0.57 eV for BChl and 0.39 eV for BChl-2w.

(14) Song, H.; Reed, C. A.; Scheidt, W. R. *J. Am. Chem. Soc.* **1989**, *111*, 6867.

density of the HOMO orbital. This gives rise to negative spin populations at all four nitrogens and also at the methine carbon atoms C5, C10, C15, and C20. These in turn give rise to the negative isotropic hyperfine couplings calculated for these positions in Table 3. In contrast to the BChl models, ligation produces large variations both in spin populations and hyperfine couplings for the Chl models. For Chl-1w$^{\bullet+}$ the spin populations of N23 and N24 are significantly decreased, and the C15 spin population changes from negative to positive compared with the nonligated Chl$^{\bullet+}$. For Chl-2w$^{\bullet+}$ even larger variations are noted with both the spin populations on N23 and N24 now being positive, resulting in correspondingly positive $^{14}$N isotropic hyperfine coupling constants, Table 3. These variations in spin populations and hyperfine couplings induced by ligation for the Chl models can again be interpreted as a reflection of a mixed orbital state for the ligated pigments. The electron density of the unperturbed HOMO-1 orbital is concentrated at the nitrogen and methine carbon atom positions, Figure 4b. Admixing of this orbital with the HOMO can therefore be expected to predominantly alter the nitrogen and methine carbon spin populations and hyperfine couplings. While such a mixed state could be clearly deduced from the geometry changes occurring on oxidation of Chl-2w, see above, the spin density data confirm that single ligation of the central Mg with a water molecule also induces orbital mixing, although to a smaller extent than the doubly ligated state.

The $^{14}$N and $^{25}$Mg isotropic hyperfine couplings for the bacteriochlorophyll models of Table 3 are in good agreement with those reported for bacteriochlorophyll *a* in liquid solution.[15] No $^{14}$N or $^{25}$Mg isotropic hyperfine couplings have thus far been reported for chlorophyll *a* in the liquid solution phase. It is likely that for chlorophyll *a* the substituent groups absent in our models of Figure 2 will have a significant effect on the extent of orbital mixing and hence may lead to variations in the $^{14}$N hyperfine and $^{25}$Mg couplings. More extended models are currently being investigated to systematically monitor such effects.

While it has been suggested in the earlier literature that admixed states were likely for chlorophyll cation radicals,[5,7] such mixed states were recently challenged by Käss et al.[15] who dismissed their relevance to chlorophyll cations in vivo and in vitro. Käss et al.[15] based their conclusions on the apparent invariance of measured $^{1}$H hyperfine couplings to substitution of the central Mg with Zn and the substitution of the 3-vinyl and the 13$^{2}$-carbomethoxy group. As the 3-vinyl group was replaced by the similar acetyl group, none of these modifications would be expected to lead to admixing. Crucially Käss et al.[15] did not vary the ligated state of the chlorophyll molecule which this and previous studies on porphyrin and chlorin radicals[5,11] have shown to be a key factor influencing admixing.

Table 3 also gives a measure of the changes in $^{14}$N couplings expected for a mixed orbital model. This is important as previous experimental ENDOR studies on the purple bacterium, *Rhodobacter sphaeroides*[17,18] and more recently for P700$^{\bullet+}$ in Photosystem I[10] used the $^{14}$N/$^{15}$N hyperfine couplings measured in vivo to eliminate a mixed orbital model for the primary donor cation free radical. In these studies it was assumed that the nitrogen hyperfine couplings should be substantially increased in magnitude by orbital mixing. Contrary to these assumptions, Table 3, shows that orbital mixing results in an actual decrease in the magnitude of most of the $^{14}$N hyperfine couplings. Hence, it is not justified to eliminate the mixed orbital state for the primary donor cation radicals on the basis of the magnitude of the measured nitrogen hyperfine couplings.

**Supporting Information Available:** Optimized Cartesian coordinates in angstroms and total energies in hartrees (PDF). This material is available free of charge via the Internet at http://pubs.acs.org.

JA010522U

(15) Käss, H.; Lubitz, W.; hartwig, G.; Scheer, H.; Noy, D.; Scherz, A. *Spectrochim. Acta* **1998**, Part A 54, 1141.

(16) Käss, H.; Rautter, J.; Zweygart, W.; Struck, A.; Scheer, H.; Lubitz, W. *J. Phys. Chem.* **1994**, *98*, 354.

(17) Lubitz, W.; Isaacson, R. A.; Abresh, E. C.; Feher, G. *Proc. Natl. Acad. Sci. U.S.A.* **1984**, *81*, 7792.

(18) Feher, G. *J. Chem. Soc., Perkin Trans. 2* **1992**, *11*, 1861.